JACS
JOURNAL OF THE AMERICAN CHEMICAL SOCIETY
Article
pubs.acs.org/JACS

Graded Structural Polymorphism in a Bacterial Thermosensor Protein

Abhishek Narayan,[†] Luis A. Campos,[‡] Sandhya Bhatia,[§] David Fushman,[∥] and Athi N. Naganathan*[,†]

[†]Department of Biotechnology, Bhupat & Jyoti Mehta School of Biosciences, Indian Institute of Technology Madras (IITM), Chennai 600036, India

[‡]National Biotechnology Center, Consejo Superior de Investigaciones Científicas, Darwin 3, Campus de Cantoblanco, 28049 Madrid, Spain

[§]National Centre for Biological Sciences (NCBS), Tata Institute of Fundamental Research, Bangalore 560065, India

[∥]Department of Chemistry and Biochemistry, Center for Biomolecular Structure and Organization, University of Maryland, College Park, Maryland 20742, United States

Supporting Information

ABSTRACT: Thermosensing is critical for the expression of virulence genes in pathogenic bacteria that infect warm-blooded hosts. Proteins of the Hha-family, conserved among enterobacteriaceae, have been implicated in dynamically regulating the expression of a large number of genes upon temperature shifts. However, there is little mechanistic evidence at the molecular level as to how changes in temperature are transduced into structural changes and hence the functional outcome. In this study, we delineate the conformational behavior of Cnu, a putative molecular thermosensor, employing diverse spectroscopic, calorimetric and hydrodynamic measurements. We find that Cnu displays probe-dependent unfolding in equilibrium, graded increase in structural fluctuations and temperature-dependent swelling of the dimensions of its native ensemble within the physiological range of temperatures, features that are indicative of a highly malleable native ensemble. Site-specific fluorescence and NMR experiments in combination with multiple computational approaches—statistical mechanical model, coarse-grained and all-atom MD simulations—reveal that the fourth helix of Cnu acts as a unique thermosensing module displaying varying degrees of order and orientation in response to temperature modulations while undergoing a continuous unfolding transition. Our combined experimental−computational study unravels the folding-functional landscape of a natural thermosensor protein, the molecular origins of its unfolding complexity, highlights the role of functional constraints in determining folding-mechanistic behaviors, and the design principles orchestrating the signal transduction roles of the Hha protein family.

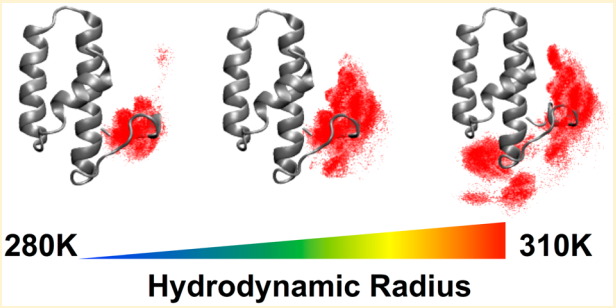

INTRODUCTION

Environmentally regulated gene expression is a fundamental repertoire of cellular systems and is particularly critical for bacteria. This enables their survival under a variety of conditions that include extremes in temperature, pH, osmolarity and nutrient availability. Specifically, a shift from ambient temperature to ∼310 K (the body temperature of the host) upon infection is a strong time-invariant signal that is exploited by several pathogens for controlled expression of virulence genes.[1] Thermosensing is orchestrated at the level of macromolecules with diverse underlying molecular mechanisms. Nonprotein based thermosensing includes temperature-modulated changes in the supercoiling status or bending of DNA, tuning the degree of structure and equilibria between closed and open forms of both cis- and trans-acting RNA elements and regulation of phosphorylation through alterations in membrane fluidity.[1−4] These molecular events in isolation or in combination with other factors eventually result in the repression or expression of genes—heat shock or virulence—in a finely tuned manner.

Protein-based thermosensing primarily involves a mechanism wherein either the oligomerization (hetero- or homo-oligomers) status or the structure of the monomers in the oligomers themselves change with temperature.[1−3] A classic example is TlpA from *Salmonella typhimurium* that undergoes a monomer to coiled-coil equilibrium upon shifts in temperature.[5] GmaR, from *Listeria monocytogenes* (a food-borne pathogen), has been shown to shift from a partially folded state to a fully unfolded state in the temperature range between 296 and 308 K.[6] In this regard, proteins of the conserved Hha-family from enterobacteriaceae serve as an interesting case.[7,8] They are small single-gene products of ∼70 residues in length, monomeric and possess a unique four-helix bundle topology

Received: October 10, 2016
Published: December 19, 2016

DOI: 10.1021/jacs.6b10608
J. Am. Chem. Soc. 2017, 139, 792−802

(Figure 1A).[9−13] Bacterial strains with *hha* deletions or null mutants display temperature-independent expression of hemolysin and other toxins indicating that Hha is critical for virulence.[14,15]

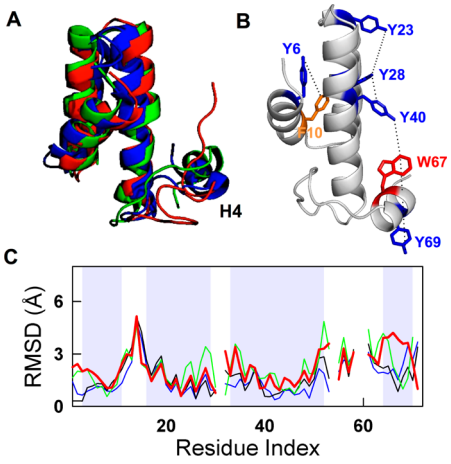

Figure 1. (A) Superimposition of Hha (blue; PDB id: 1JW2), YmoA (green; 2K5S) and Cnu (red; 2JQT) NMR models at 295 K. The helix H4 is partially structured in Cnu at this temperature. (B) Cartoon highlighting the distances between the various aromatic residues in Cnu (black lines). The distances are (in Å units): Y6/F10−7.4; F10/Y28−8.5; Y23/Y28−10; Y28/Y40−4; Y40/W67−5.8; W67/Y69−13.6. (C) Residue-wise C_α RMSD for the Hha-family members with respect to 1JW2:2MW2 (blue), 2K5S (green) and the folded conformation of Cnu (red) modeled with the Robetta server[21] using 1JW2 as a template. The shaded regions correspond to the secondary structure elements H1 to H4. The Hha-sequence is longer than YmoA and Cnu resulting in gaps in the structural alignment.

Hha-like proteins modulate the expression of virulence factors by forming a complex with the oligomeric transcription repressor H-NS,[16,17] which is located at the crossroads of several genetic regulatory circuits and controls the expression of nearly 69% of thermo-regulated genes.[18] The expression of toxins is silenced by the H-NS−Hha complex at low temperatures (280−293 K) while they are enhanced by up to an order of magnitude at the physiological temperature of 310 K.[8,19,20] They further display a temperature-dependent proteolytic cleavage within cells suggestive of a tunable stability profile within the physiological range of temperatures (<310 K).[22] These experiments reveal that Hha-like proteins act as molecular thermosensors.

Despite these experiments, the precise molecular determinants and mechanism of thermosensing by Hha-like proteins and hence the pathogenic response are currently unclear. Given the intrinsically flexible nature of single-domain helical proteins, several possible signal-transducing mechanisms could be envisaged in Hha-like proteins: a temperature-dependent equilibrium between two states with different conformations and varying binding affinities to H-NS (a molecular switch between folded and unfolded or intermediate states), a continuous transition between substates that allows for a graded response to extrinsic stimuli (a molecular rheostat), or a conformational behavior that can be coarsely described as being intermediate to the two scenarios above.[23] From a folding mechanistic perspective, the possibilities discussed above correspond to two-state or multistate,[24−26] one-state[27] and marginal-barrier systems,[28−30] respectively, that can be discerned from multiprobe spectroscopic studies.[27,31−39] Temperature-modulated structural changes can also be concentrated on the folding side of the main barrier that separates the native ensemble from the unfolded ensemble. This could potentially occur when only a part of the protein undergoes thermally induced structural changes while the rest of the structure acts as a scaffold, a mechanism that has not been observed before.

To explore these questions, we study Cnu (or YdgT),[40] one of the members of Hha-family that can substitute for Hha in vivo without any adverse effects to the cell.[41] Though the sequence of Cnu shares high similarity and moderate identity with Hha (67% and 38%, respectively), the published NMR structure of Cnu indicates that the fourth helix is only partially structured at 298 K.[11] This helix is well folded in Hha and its close homologue YmoA from *Yersinia enterocolitica* that share 93% sequence similarity.[9,10] An analysis of all published structures from this family (at ∼295 K) indicates a clear difference in the relative position of the fourth helix and the long loop preceding it, both in the presence or absence of H-NS (Figure 1C; 2MW2 is solved in the presence of H-NS). We hypothesize that this unique feature, i.e., conformational flexibility in the fourth helix, determines the thermosensing behavior of Cnu.

In the current work, we explore the molecular origins of thermosensing by Cnu employing experimental spectroscopic, calorimetric, hydrodynamic methods and NMR. We then rationalize our experimental findings through a computational study that includes statistical mechanical modeling, coarse-grained and all-atom MD simulations. We effectively show that the varied approaches are mutually consistent with each other and provide, to our knowledge, the first detailed folding-function landscape of a natural thermosensor protein.

MATERIALS AND METHODS

Purification Protocol. The gene of Cnu corresponding to the protein sequence MKEKEMTVQDYLLKFRKISSLESLEKLYDH-LNYTLTDDQELINMYRAADHRRAELVSGGRLFDLGQVPKSVW-HYVQEKEK was cloned in pTXB1 vector (New England Biolabs) to generate fusion product of Cnu-Mxe-GyrA-intein-CBD (chitin binding domain) and transformed into *E. coli* BL21 Star (DE3) (Invitrogen). The four-residue charged tails at the N- and C-termini were added to increase the solubility of Cnu which otherwise goes primarily into inclusion bodies. The culture was grown at 37 °C to an OD of ∼0.8 and induced with 1 mM IPTG for 6 h. The cells were lysed by sonication, and the supernatant following the removal of cell debris was passed through a 5 mL chitin bead column (New England Biolabs) and washed thoroughly with 20 column volumes of column buffer (20 mM HEPES pH 8.5, 500 mM NaCl, 1 mM EDTA). Following this, the column was equilibrated with 5 column volumes of cleavage buffer (20 mM HEPES pH 8.5, 500 mM NaCl and 50 mM DTT) to initiate the intein cleavage reaction at 23 °C for 40 h. The cleaved product from the column was lyophilized, dissolved in Milli-Q water, loaded on to a size exclusion column (GE Superdex 75pg) pre-equilibrated with 150 mM ammonium acetate (pH 8.0), eluted with the same buffer and again lyophilized. The identity of the protein was confirmed by MALDI and purity was ascertained to be >98% by analytical size-exclusion chromatography. The peptide corresponding to the fourth helix together with its neighboring residues (C-pep; GRLFDLGQVPKSVWHYVQ) was purchased from Genscript, USA.

Equilibrium Spectroscopy. All experiments were carried out at pH 8.0 and in a 170 mM ionic strength buffer (20 mM phosphate buffer +112 mM NaCl). Far- and near-UV CD temperature-wavelength spectra were collected using JASCO J-815 spectrophotometer coupled to a Peltier system in 1 mm and 10 mm quartz cuvettes, respectively. Intrinsic protein fluorescence on excitation at

DOI: 10.1021/jacs.6b10608
J. Am. Chem. Soc. 2017, 139, 792−802

274 and 295 nm were recorded in a JASCO FP-6500 spectrophotometer coupled to a water-bath using a 10 mm path-length quartz cuvette. The protein quantum yields (QY) were calculated using the NATA quantum yield as a reference at 298 K and pH 7.0 (0.13). Steady-state fluorescence anisotropy was measured in Biologic MOS-450 by selectively exciting W67 at 295 nm and collecting the vertical and horizontally polarized components using an Asahi Spectra 350 nm bandpass filter.

Differential Scanning Calorimetry. DSC experiments were carried out in a Microcal VP-DSC (Malvern, UK). The protein samples were desalted in buffer and degassed at 298 K prior to loading into the calorimetric cells. The experiments were performed at three different protein concentrations in the range of ∼40−100 μM at a scan rate of 1 K/min. Several buffer−buffer baselines were acquired to ensure proper equilibration of the calorimetric cells. After protein scan, buffer−buffer baselines were again measured to ensure that there was no significant baseline drift.

Analytical Size-Exclusion Chromatography (aSEC). The Stokes radius of Cnu at 278 K was determined by analytical size-exclusion chromatography using GE Superdex 200 HR column. The column was calibrated with five different proteins (Ferritin, Aldolase, Conalbumin, Albumin, Ribonuclease) of known Stokes radii. Cnu (∼90 μM) was injected into the column and eluted with the 170 mM ionic strength buffer.

Analytical Ultracentrifugation (AUC). Cnu (∼50 μM at pH 8.0 and 170 mM ionic strength conditions) was incubated overnight at 277 K and filtered with a 0.2 μm filter. Sedimentation velocity experiments were carried out in Optima XL-I (UV−vis absorbance at 280 nm and interference detection) at 48 000 rpm and at two different temperatures, 278 and 298 K. The sedimentation velocity profiles were collected at different time intervals and the sedimentation coefficients calculated using SEDFIT with standard buffer densities and viscosities.

Nuclear Magnetic Resonance (NMR). The NMR measurements were performed for a range of temperatures, from 283 to 310 K, on Bruker Avance III 600 and 800 MHz spectrometers equipped with cryogenic probes. The NMR sample contained 80 μM ^{15}N-enriched Cnu dissolved in a 20 mM sodium phosphate buffer (pH 8.0) containing 112 mM NaCl, 5% D_2O, and 0.02% (v/v) NaN_3. A freshly prepared sample was used for each set of measurements. Heteronuclear experiments included ^{1}H−^{15}N HSQC, SOFAST-HMQC, and TROSY spectra, typically recorded with the spectral widths of 7183 Hz (^{1}H) and 1520−2068 Hz (^{15}N).

Wako-Saitô-Muñoz-Eaton (WSME) Model. The latest version of the WSME model[42,43] that includes contributions from packing interactions, solvation, electrostatics and structure-dependent entropy was employed.[44−46] The absolute heat capacity profile of Cnu was fit to WSME model using a 5 Å cutoff for heavy-atom interactions. The final parameters are entropic penalty of $\Delta S = -14.5$ J mol^{-1} K^{-1} per residue for residues identified as helical by STRIDE, $\Delta S = -20.6$ J K^{-1} mol^{-1} per residue for all other residues (i.e., a $\Delta\Delta S = 6.1$ J mol^{-1} K^{-1}), and van der Waals interaction energy per native contact $\xi = -78.9$ J mol^{-1}.

All-Atom Coarse-Grained Simulations. The coarse-grained model of Onuchic and co-workers was employed for the unfolding studies (SMOG server[47]) with a 6 Å cutoff and eliminating up to 3 nearest neighbor interactions for identifying native contacts. All other parameters and the GROMACS[48] simulation protocols are identical to that used in a recent work.[49]

Explicit-Solvent All-Atom Molecular Dynamics (MD) Simulations. The GROMACS simulation software together with the Amber-99SB*-ILDN force field was employed for exploring the conformational space sampled by Cnu. The protein was placed in a dodecahedral box with periodic boundary conditions and a minimum distance of 15 Å between the structure and the box edge. The protein was solvated with TIP3P waters along with ions to maintain charge neutrality, energy-minimized and relaxed for 2 ns at 280 K with a two-femtosecond time-step. Three independent NVT simulations of 1 μs each were run at two temperatures—280 and 310 K—with randomized starting velocities for an aggregate simulation time of 6 μs with 4 fs time-step (enabled with virtual hydrogen). A Langevin thermostat with a damping coefficient of 1/(1 ps) was employed for maintaining the temperature. Long-range electrostatics was calculated using the particle mesh Ewald (PME) procedure at grid spacing of 1.2 Å and with a 10 Å cutoff for nonbonded interactions.

RESULTS

Multiprobe Spectroscopy Reveals Complex Temperature-Induced Structural Changes. The far-UV CD spectrum of Cnu at 278 K is consistent with the expectations of a helical protein but with a reduced helicity of ∼35−39% (Figure 2A) compared to that estimated from the NMR

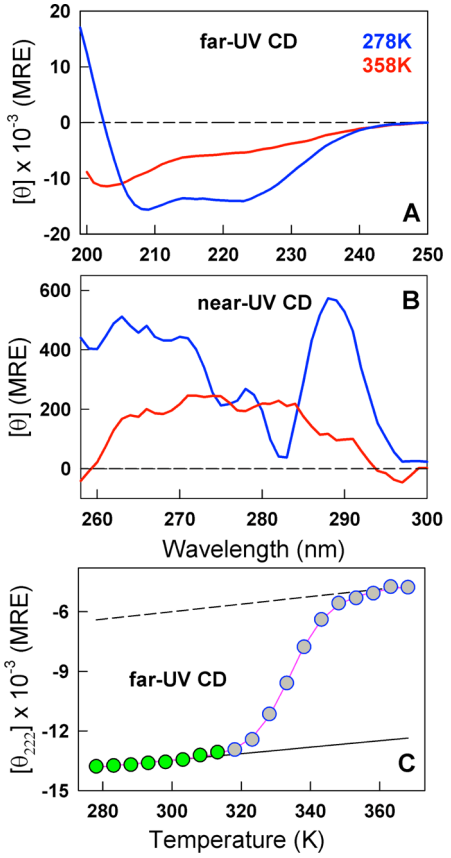

Figure 2. (A,B) Far- and near-UV CD spectra of Cnu under folding (278 K) and unfolding conditions (358 K). The spectra are reported in the mean residue ellipticity (MRE) units of deg. cm^2 dmol^{-1}. (C) Two-state fit (red) to the far-UV CD unfolding data at 222 nm (circles) together with the folded (continuous black) and unfolded baselines (dashed line). The green filled circles represent the apparently flat pretransition observed in the physiological range of temperatures.

structure (∼70%). The near-UV CD spectrum at the same temperature clearly resolves the detailed vibronic structure of the aromatic amino acids in Cnu—single tryptophan (>280 nm), 5 tyrosines (∼270−280 nm) and 2 phenylalanines (<270 nm)—indicative of a well-folded protein (i.e., Cnu is not a molten globule; Figure 2B). The tyrosines at positions 6, 23, 28 40, and 69, F10 and W67 are spatially within 10 Å of each other thus allowing for a large excitonic coupling[50] that contributes to the observed fine structure (Figure 1B). The secondary and tertiary structure fingerprints are lost at higher temperatures when monitored by both far- and near-UV CD. The far-UV CD monitored thermal unfolding curve at 222 nm presents an apparent two-state-like behavior with a flat pretransition

DOI: 10.1021/jacs.6b10608
J. Am. Chem. Soc. 2017, 139, 792−802

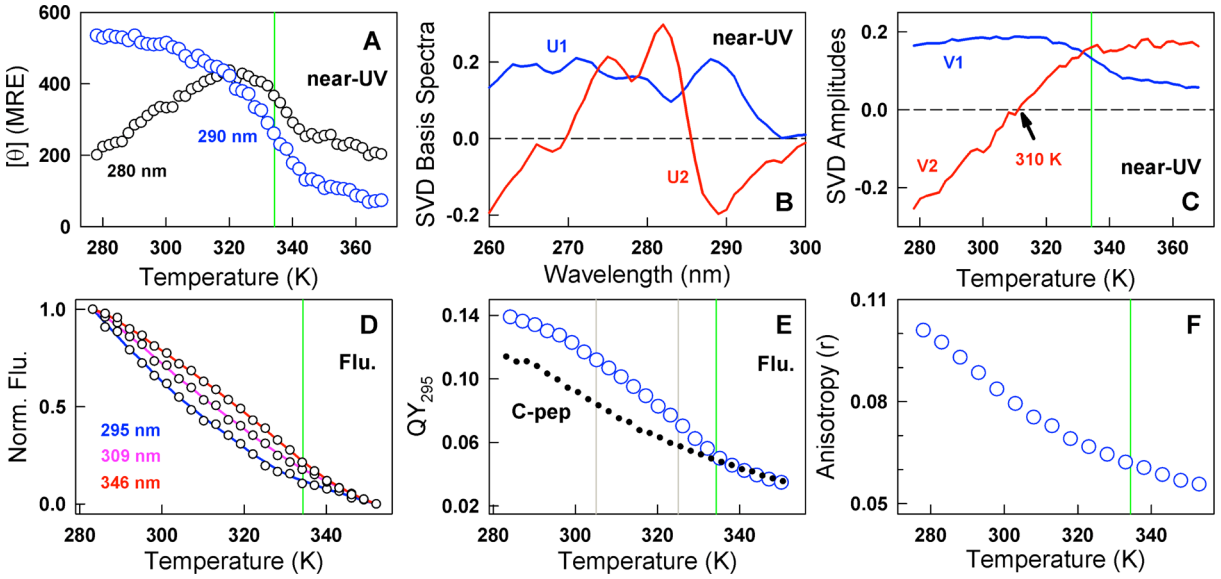

Figure 3. Probe-dependent unfolding thermodynamics. The green vertical line signals the melting temperature as measured from far-UV CD at 222 nm. (A) Representative examples of the complex unfolding thermodynamics observed by near-UV CD at two different wavelengths. (B,C) The two significant basis spectra (U1 and U2) extracted from singular value decomposition (SVD) of temperature-wavelength near-UV CD data. The corresponding amplitudes (V1 and V2) are shown in panel C. The amplitude of the second component has a near-continuous temperature dependence and exhibits a sign-change at 310 K. (D) Wavelength-dependent fluorescence emission unfolding curves observed upon exciting Cnu at 274 nm. (E) The quantum yield (QY) of the sole tryptophan in Cnu (blue) and in the peptide C-pep (black dots) derived from the C-terminal region. The gray vertical lines signal the two inflection points estimated from a first-derivative analysis of the Cnu QY temperature dependence. (F) Tryptophan anisotropy as a function of temperature.

baseline, a melting temperature of ~334 K and an unfolding enthalpy at the midpoint of 177 kJ mol^{-1} (Figure 2C). The fitting errors in T_m and ΔH_m for two-state fits to far-UV CD data and other probes discussed below are ±0.2−0.5 K and ±3−6 kJ mol^{-1}, respectively. The unfolding enthalpy per residue amounts to ~2.4 kJ mol^{-1} which is significantly lower than the 2.9 kJ mol^{-1} per residue scaling expected for single-domain proteins.[51] This is suggestive of weak energetic coupling within the structure that is generally observed in proteins with low cooperativity.

The apparent lack of structural changes (i.e., the flat pretransition) when monitored by far-UV CD between 280 K −310 K is surprising, as conformational changes in Cnu have been implicated in regulating the binding to H-NS in the same range of temperatures. How then does Cnu sense the temperature changes? To answer this question, we performed a detailed multiprobe spectroscopic study.[27,52] Thermal unfolding when probed by near-UV CD, which reports on the tertiary environment of aromatic amino acids, reveals distinct wavelength dependence. At 290 nm, the unfolding profile looks similar to far-UV in terms of the inflection point (~333.5 K) but with a steeper pretransition (Figure 3A). The two-state unfolding enthalpy for this transition is therefore only ~130 kJ mol^{-1} which is more than 40 kJ mol^{-1} lower than that from far-UV CD. The unfolding curve at 280 nm is dramatically different from that at 290 nm and exhibits a trend where the signal increases, reaches a maximum at ~320 K, and then decreases with temperature (black in Figure 3A).

Since the tertiary structure changes are complex and wavelength-dependent, we performed a spectral deconvolution of the temperature-wavelength near-UV CD data by Singular Value Decomposition (SVD). SVD identifies two significant components (basis spectra) with the first component U1 representing the average spectrum and whose amplitude V1 resembles that of a typical two-state-like unfolding curve with a flat pretransition (Figure 3B,C). The second basis spectrum U2 interestingly points to an anticorrelation between the spectral bands of tyrosine and tryptophan (Figure 3B). The amplitude V2 changes continuously with temperature (i.e., no pretransition) with a sign change at 310 K. Moreover, the change in tertiary packing environment observed by this component is 100% complete at the global T_m of 334 K (Figure 3C). The interplay between these two components and amplitudes is the origin of the complex wavelength-dependent unfolding equilibria in Cnu.

Wavelength dependence of unfolding thermodynamics is also observed in fluorescence experiments upon excitation of Cnu at 274 nm. The normalized emission fluorescence intensities as a function of temperature are broad and display steep temperature dependence irrespective of the wavelengths (Figure 3D). We then selectively probed for the behavior of the sole tryptophan (W67) in the fourth helix by exciting Cnu at 295 nm (Figure 3E). If W67 is buried within the nonpolar protein interior it is expected to mimic the unfolding profile of far-UV CD (if the intrinsic temperature dependence is accounted for) and importantly exhibit an emission maximum (λ_{max}) at ~320 nm.[53] However, we find that the fluorescence emission maximum of W67 is red-shifted to 346 nm implying a polar environment around the tryptophan (Figure S1A). To account for any local structural effects that could modulate the λ_{max} of W67, we performed similar experiments on a disordered peptide derived from the fourth helix (C-pep; see Materials and Methods and Figure S2) and find that the emission maximum of the tryptophan occurs at ~352 nm (Figure S1A). These observations indicate that W67 is only partially buried while still making nonlocal contacts.

The tryptophan in C-pep shows a near-linear decrease in its quantum yield (QY) as a function of temperature. On the other

DOI: 10.1021/jacs.6b10608
J. Am. Chem. Soc. 2017, 139, 792−802

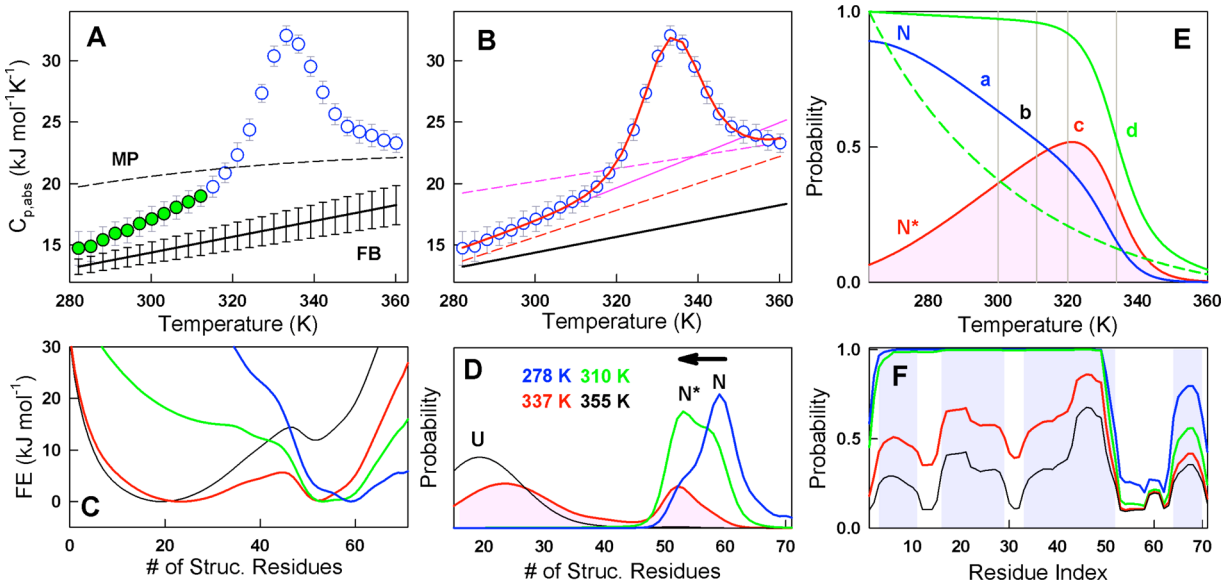

Figure 4. Structurally heterogeneous native ensemble in Cnu and the molecular origins of unfolding complexity. (A) Absolute heat capacity of Cnu (circles) together with the Freire folded baseline (FB) and the Makhatadze-Privalov (MP) unfolded baseline. The green circles highlight the temperature regime where far-UV CD exhibits little structural change. (B) Crossing baselines from a two-state fit (magenta) and the baseline from the WSME model analysis of the Cnu thermogram (dashed red). The fit from the WSME model is shown in red together with the Freire baseline (black). (C,D) One-dimensional free-energy profiles and the corresponding probability densities at select temperatures. Note that the native state, N, is in equilibrium with a partially structured state N*. (E) Temperature-dependent changes in population of N and N* resemble the experimental signal changes in the QY of W67 and near-UV CD at 280 nm. The points a, b, c and d represent the temperatures at which the minor unfolding transition is observed in QY measurements (Figure 3E), the sign changes in the SVD analysis of near-UV CD data (~310 K; Figure 3C), the 280 nm near-UV CD unfolding curve peaks (~320 K; Figure 3A), and the major inflection point is observed by CD and DSC (~334 K), respectively. The normalized mean residue-unfolding probabilities are also shown for the first 50 residues (continuous green) and the last 20 residues of Cnu (dashed green lines). The latter resembles the temperature dependence of fluorescence emission intensity upon excitation at 274 nm (Figure 3D). (F) Probability of a residue being folded highlighting the distribution of local stability across the sequence as predicted by the WSME model. Blue shades represent α-helical segments.

hand, the temperature dependence of W67 quantum yield (i.e., the protein) is weakly cooperative and very different from that of C-pep suggesting that the difference originates from nonlocal interactions (most likely with the C-terminal half of helix 3; Figure 3E). Interestingly, two transitions are evident in the first-derivative analysis with apparent minor and major inflection points at 305 and 325 K, respectively, both of which are lower than the estimates from far- and near-UV CD (Figure S1B). It is still possible to fit this unfolding curve to a two-state model (with an unfolded baseline derived from the C-pep to account for intrinsic temperature effects). Such an exercise results in a lower T_m of 330.7 K and an unfolding enthalpy of ~90 kJ mol^{-1}, which is just ~50% of the Cnu unfolding enthalpy estimated by far-UV CD (Figure S1C). Steady-state anisotropy (r) of W67 also reveals the lack of a flat pretransition and decreases sharply with temperature. r is a function of the fundamental anisotropy (r_0), excited state lifetime of W67 and the rotational correlation time of the molecule,[53] all of which (together or in isolation) are highly sensitive to the environment around W67. Also, the rotational correlation time is a measure of the shape of the molecule that can be modulated by partial unfolding events. Taken together, the decrease in fluorescence QY and the steep change in steady state anisotropy between 280 and 310 K is strong evidence that structural changes occur in the pretransition region.

Multiprobe spectroscopic analysis of Cnu unfolding effectively reveals a large spread in apparent melting temperatures (305−334 K) and unfolding enthalpies (90−177 kJ mol^{-1}), despite the far-UV CD pointing to a two-state-like system. Moreover, we find that the structure melts earlier (i.e., at a lower temperature) in regions of the fourth helix from fluorescence experiments. Changes in packing also occur at lower temperatures (near-UV CD) well before the global unfolding indicative of a system that is highly sensitive to temperature changes.

Scanning Calorimetry Experiments Point to Temperature-Dependent Malleable Native Ensemble in Cnu. The probe-dependent unfolding of Cnu is similar to well catalogued observations in downhill folding proteins.[27,34,37,54,55] In such systems, Differential Scanning Calorimetry (DSC) measurements provide a direct avenue to quantify folding cooperativity and hence the thermodynamic barrier height.[54,56,57] Moreover, because heat capacity is a measure of enthalpic fluctuations, it allows for an objective analysis of the global thermodynamics and structural fluctuations independent of any specific probe.[54,58,59]

Figure 4A plots the absolute heat capacity profile ($C_{p,abs}$) of Cnu derived from protein concentration dependence of apparent heat capacity as prescribed before[60] (also see Figure S3). A simple procedure to check for the accuracy of the generated DSC data is to compare it to published empirical predictions for folded and unfolded states of proteins.[61] Particularly, the Freire Baseline (FB) is an empirical measure of the magnitude and temperature dependence of heat capacity for well-folded proteins.[62] Any deviations from the behavior predicted by the FB, specifically at temperatures below the transition midpoint, are predictive of structural changes. In this regard, we find that the pretransition heat capacity of Cnu

DOI: 10.1021/jacs.6b10608
J. Am. Chem. Soc. 2017, 139, 792−802

approaches the FB at low temperatures (<280 K) indicating that the protein is well folded under these conditions. However, the heat capacity exhibits a steeper slope than that observed for well-folded single domain proteins, hinting that the structure of Cnu starts melting even at the physiological range of temperatures (highlighted by green circles in Figure 4A) in agreement with other spectroscopic probes. The changes in pretransition are even more stark when compared with Ubq,[63] a similarly sized-protein that exhibits little conformational change in the same range of temperatures (Figure S4).

The heat capacity profile of Cnu can still be fit to a two-state model with a T_m of ∼334 K and an unfolding enthalpy of ∼195 kJ mol^{-1}. Such a fit is however physically unreasonable as the folded and unfolded baselines cross within the experimental temperature range (magenta in Figure 4B). Similar crossing of baselines are also seen in global two-state or three-state models (with 22 and 34 parameters, respectively) that result in cold denaturation, not observed experimentally (Figure S5, S6). This is evidence that an ensemble description, rather than a discrete macrostate analysis, is more appropriate to characterize the heat capacity profile of Cnu.

Accordingly, we analyze the absolute heat capacity data employing the residue-level ensemble-based Wako-Saitô-Muñoz-Eaton (WSME) model.[42,43] In the current work, we employ the latest version of the WSME model that includes contributions from packing, solvation, electrostatics and structure-dependent entropy (see Materials and Methods).[44−46] We obtain a very good fit with the WSME model albeit with a folded baseline that is close to the FB + 1σ baseline (Figure 4B). The estimated barrier height at the midpoint is ∼5 kJ mol^{-1} suggestive of a marginal barrier system. The free energy profile is downhill-like at low temperatures (<310 K) with a broad and structurally heterogeneous native ensemble under physiological conditions (310 K; green in Figure 4C). The native ensemble is predicted to be composed of two subpopulations, N (fully folded state) and N*, that are separated by near-zero thermodynamic barrier (Figure 4D; maximal barrier <0.2 kJ mol^{-1}). The two "states" exchange populations in a temperature dependent manner with each other at low temperatures (<320 K) and with the fully unfolded state at temperatures >320 K (Figure 4E).

The shape of unfolding as monitored by population change of N resembles the QY of W67 with two apparent transitions (compare blue in Figure 4E with Figure 3E) and that of N* resembles that of the near-UV CD signal at 280 nm (compare red in Figure 4E with Figure 3A). The change in sign of the near-UV CD signal at 310 K therefore occurs at a temperature at which N* starts to dominate over N (point b in Figure 4E). Residue unfolding probabilities (Figure 4F) reveal the structural features of N*—a state in which the fourth helix is only partially structured or unfolded. W67 is therefore sensitive to both the local unfolding of the fourth helix and the rest of the structure (see Figure 1B). This in turns contributes to the low unfolding enthalpy and melting temperature when probed by fluorescence techniques. In fact, mean residue-unfolding probabilities of the region after the third helix results in a temperature dependence that is very similar to the fluorescence emission upon excitation at 274 nm (compare Figure 3D with green dashed line in Figure 4E). The WSME model thus provides a clear structural-energetic connection while simultaneously revealing the molecular origins of the observed experimental unfolding complexity (Figure 3).

Evidence for Increase in Stokes Radius in the Pretransition Region from Hydrodynamic Measurements. Spectroscopic and calorimetric measurements reveal that the tertiary structure of Cnu melts even within the pretransition region of the far-UV CD experiment. If the structure does melt and if it arises from the melting of the fourth helix, the effective volume of the protein is expected to concomitantly increase. We therefore resorted to hydrodynamic measurements[64,65] to quantify this phenomenon directly.

Analytical size-exclusion chromatography (aSEC) at 278 K resulted in a single and well-resolved elution profile confirming that the protein is a monomer under conditions of our experiments (Figure 5A). Using a standard graph of 5 proteins

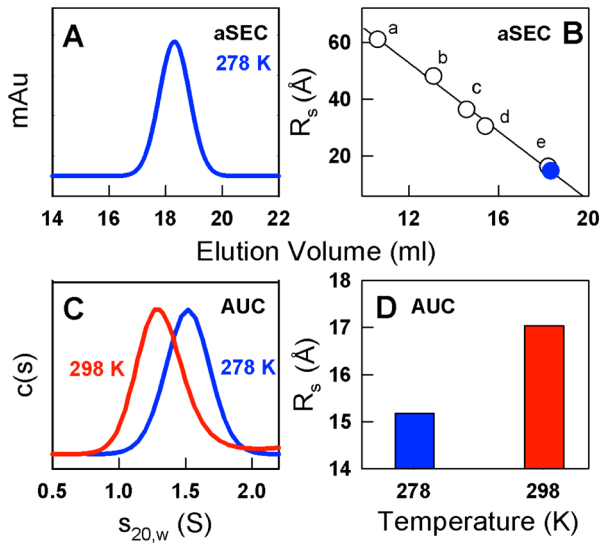

Figure 5. Direct observation of structural swelling in the native ensemble. (A) The elution profile of Cnu from analytical size exclusion chromatography (aSEC) at 278 K. (B) The standard graph used to estimate the Stokes radius (R_S) of Cnu (blue). The reference proteins with known Stokes radii are a, Ferritin; b, Aldolase; c, Conalbumin; d, Albumin; e, Ribonuclease. (C,D) The sedimentation-coefficient distributions (in units of Svedberg, S) from analytical ultracentrifugation (AUC) at 278 (blue) and 298 K (red) and the corresponding Stokes radii (panel D).

with known Stokes radii (R_S) and elution volumes, we establish the R_S of Cnu to be 14.9 Å at 278 K (blue in Figure 5B). Analytical ultracentrifugation (AUC) at the same temperature revealed a single uniformly sedimenting species with an apparent *s*-value of 1.52 S ($s_{20,w}$) and a Stokes radius of 15.2 Å in excellent agreement with aSEC (Figure 5C). At 298 K, the c(s) distribution shifts to lower values with an apparent $s_{20,w}$ of 1.31 S suggesting an increase in the frictional factor compared to 278 K. This increase in frictional factor translates to a Stokes radius of 17.0 Å at 298 K, corresponding to an increase in protein volume of ∼40% compared to 278 K (assuming a spherical particle; Figure 5D).

Structural Polymorphism from NMR Experiments. The experiments detailed above point to substantial conformational heterogeneity in the native ensemble of Cnu. However, they probe only the coarse features of the folding landscape. To explore if such polymorphism is also observed at the atomic-level, we performed NMR experiments with ^{15}N-labeled Cnu. The ^{1}H−^{15}N correlation spectra of Cnu show well-dispersed

DOI: 10.1021/jacs.6b10608
J. Am. Chem. Soc. 2017, 139, 792−802

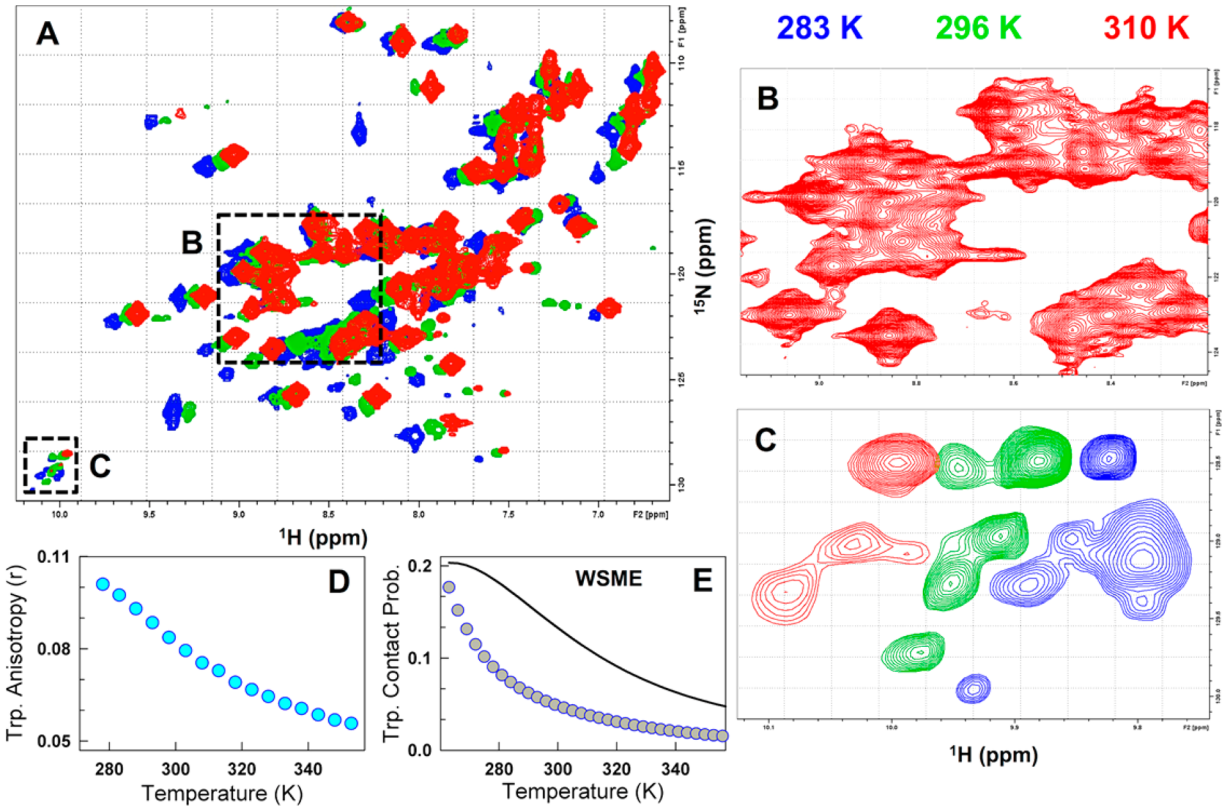

Figure 6. Conformational heterogeneity in the pretransition region of Cnu from NMR. (A–C) Overlay of ^{1}H–^{15}N HMQC spectra at 283 K (blue), 296 K (green) and 310 K (red), respectively. (B) Blow-up of the central region of the spectrum at 310 K highlighting the presence of multiple protein conformations in slow exchange. (C) The tryptophan indole region of the spectra shown without compensation for the temperature shift of the lock signal for the sake of visual clarity. (D) Steady-state anisotropy (upon excitation of W67 at 295 nm) decreases sharply with temperature supporting the observations in panel C. (E) WSME model predictions of changes in tryptophan contact probability with the rest of the residues in the protein (circles) and the associated standard deviation (line) are in accordance with NMR observations.

amide signals indicative of a reasonably folded protein at all temperatures studied (Figure 6A). However, a closer inspection reveals several peaks clustered around the same location in the spectrum, suggesting the presence of several protein conformations in slow exchange (on the NMR time scale) with each other (Figure 6B). The heterogeneity observed throughout the NMR spectra is in agreement with near-UV CD that points to complex modulations of the tertiary structure at temperatures ≤310 K (Figure 3A–C).

Since tryptophan indole resonances are observed at a specific region of the ^{1}H–^{15}N HMQC spectrum (>9 ppm in ^{1}H and >120 ppm in ^{15}N), we can directly probe for conformational changes in the fourth helix (where W67 is located) without a detailed NMR signal assignment. Remarkably, we observe the presence of 5–6 resonances corresponding to W67 (specifically the indole NH-group of W67, W67ε) even at the lowest temperature (283 K; blue in Figure 6C). It is important to note that only a single resonance is expected for a tryptophan in a well-folded environment. The observation of numerous resonances strongly suggests that W67 samples multiple long-lived conformational states despite being located in an asymmetric environment (Figure 2B for the near-UV CD spectrum). Specifically, the closest distance between the W67ε peaks (at each temperature) in the spectra shown in Figure 6C is $\Delta\omega/2\pi \approx 20$ Hz, which means that the exchange time scale must be much slower than 8 ms (exchange rate, $k_{ex} < 125\ s^{-1}$). This heterogeneity appears to decrease at higher temperature (fewer observed resonances; green and red in Figure 6C), likely reflecting enhanced exchange between conformational states or due to unfolding that reduces chemical heterogeneity.

In fact, steady-state anisotropy measurements reveal that the environment of W67 becomes less anisotropic rapidly with temperature due to partial unfolding (Figure 3F, 6D). The WSME model predictions further indicate that the mean contact probability of W67 with other residues in the protein and the associated standard deviation decrease with temperature (circles and line in Figure 6E, respectively). These complementary observations indicate that W67, and by extension the short fourth helix, display conformational heterogeneity arising from unfolding at temperatures ≤310 K consistent with interpretations from fluorescence and near-UV CD probes.

Simulations Provide a Consistent Explanation to the Varied Experimental Observations. To further validate the experimental observations of complex structural changes in Cnu we performed all-atom coarse-grained (CG) simulations (Materials and Methods). We find a continuous increase in the radius of gyration of Cnu at low temperatures well before the melting temperature in agreement with hydrodynamic experiments (Figure 7A). Decoupling the pairwise residue contact space into two sets, one set of interactions that includes all interactions within the first three helices and another set that includes all inter- and intra(loop + helix 4) interactions, we find that the latter changes significantly earlier (thermodynamically) and exhibits lower T_m (Figure 7A,B). Two transitions are evident in the unfolding of this region mirroring fluorescence

DOI: 10.1021/jacs.6b10608
J. Am. Chem. Soc. 2017, 139, 792–802

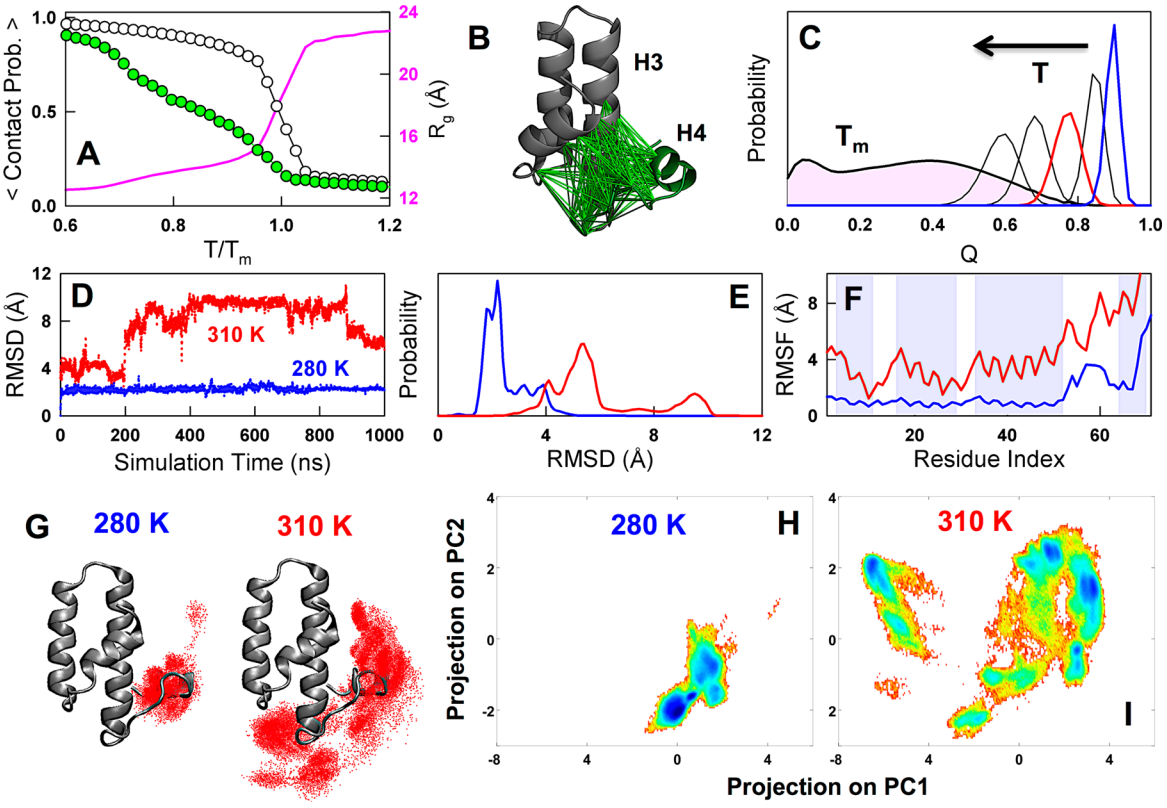

Figure 7. Structural polymorphism in Cnu from atomistic simulations. Panels A–C and D–I highlight the results of coarse-grained and all-atom molecular dynamics simulations, respectively. (A,B) Panel A plots the increase in the radius of gyration (R_g; magenta) as a function of reduced temperature from all-atom coarse-grained simulations. Note that R_g increases continuously well before the unfolding midpoint. Temperature dependent mean contact probabilities of all interactions within the first three helices and between helix 4 and the rest of the structure (green in panel B) are shown in black and green circles, respectively, in panel A. (C) One-dimensional probability densities as a function of the fraction of native contacts (Q) at increasing temperatures (arrow) highlighting the gradually unfolding native ensemble that crosses a marginal barrier at the midpoint. (D) Representative one-microsecond long all-atom MD trajectories at 280 and 310 K. (E,F) C_α RMSD distribution and root-mean-square-fluctuation (RMSF) plots from the three trajectories at both the temperatures. The shaded areas in panel F signal the secondary structure elements. (G) Structural changes in the region following the third helix of Cnu at 280 and 310 K viewed from the perspective of C_α of W67 that is located in the fourth helix (red dots; generated by concatenating all the trajectories at a particular temperature). (H,I) Free-energy landscape of Cnu from a global principal component (PC) analysis of 6 μs of cumulative simulation time. The landscape is colored in the spectral scale from low free energy (blue) to high free energy (red).

experiments that probe the environment of W67 (Figure 3E). The loss of interactions involving the fourth helix is nearly complete even before the T_m of the main transition in accordance with near-UV CD spectral analysis. These results are confirmation that structural changes observed at low temperatures in experiments originate from the melting of the contacts involving the fourth helix and its neighbors. The CG simulation also predicts that the disorder in the fourth helix increases in a continuous manner—note the native ensemble movement in the one-dimensional projections of Figure 7C. Remarkably, a similar observation can be extracted from a variable-barrier model analysis[54] of the heat capacity profile of Cnu (Figure S7).

While we observe a remarkable level of agreement between experiments and the CG simulations, it is well-known that the temperature scales are not directly comparable.[66] We therefore performed additional simulations in explicit solvent at more realistic temperatures of 280 and 310 K (6 μs of aggregate simulation time; see Materials and Methods and Figure 7D, S8). The expectation is to identify regions of structure that are thermodynamically less stable despite the expected differences in sampling between temperatures that are 30 K apart. At 280 K, we observe small but significant structural changes in the fourth helix and in the long loop that connects it to the third helix. The intrinsic dynamics in the fourth helix exposes W67 to the polar solvent environment and to the polar side chains in the third helix (particularly R41 and D44) that in turn manifests as a red-shifted spectrum in fluorescence emission experiments. Apart from this region, Cnu displays little dynamics with minimal fluctuations throughout the structure (Figure 7E and 7F). This is in accordance with the independent observation that the low temperature heat capacity approaches the Freire baseline (indicative of minimal enthalpic fluctuations; Figure 4A).

As the temperature is increased to 310 K, the RMSD distribution shifts toward higher values (Figure 7E). This temperature-dependent change is not concentrated on just the fourth helix but encompasses the entire structure (Figure 7F). These enhanced structural fluctuations are consistent with the steep pretransition slope observed in heat capacity measurements. The fourth helix is only partially structured in this range of temperatures while simultaneously making extensive transient non-native interactions with helix 3 that is highlighted from the perspective of W67 in Figure 7G. These specific structural changes are the molecular origins of the increasing Stokes radii with temperature and are in accordance with the

DOI: 10.1021/jacs.6b10608
J. Am. Chem. Soc. 2017, 139, 792–802

interpretation of fluorescence experiments, WSME model and CG simulation predictions.

A global principal component analysis (PCA) of the trajectories reveals multiple minima at 280 K (dark blue in Figure 7H). These represent the various conformational substates of Cnu differing primarily in relative orientation of W67 mirroring NMR observations at low temperature. There is a large increase in the conformational space sampled by Cnu at 310 K compared to 280 K (Figure 7I) arising from the melting of the fourth helix.

DISCUSSION

Numerous biochemical experiments have highlighted the critical role played by Hha family members (one of which is Cnu) in modulating the expression of virulence genes in response to temperature changes. However, little biophysical evidence exists as to how thermal perturbations are transduced to conformational changes. In the current work, we explore this open question employing the protein Cnu from *E. coli* as a model system. We characterize the structural response of Cnu to thermal stress employing a variety of experimental techniques that probe distinct features, all of which reveal complex conformational changes in the physiological range of temperatures. These observations raise questions on the nature of the folding mechanism that couples the response of Cnu to thermal stress.

In this regard, the argument for a non-two-state transition in Cnu can be made qualitatively without resorting to models. For example, we observe complex unfolding patterns in near-UV CD (Figure 3), increase in dimensions of the native ensemble from AUC (Figure 5) and substantial conformational heterogeneity by NMR (Figure 6). These observations cannot be explained as arising from an interconversion between folded and unfolded states simply because they are observed even at lower temperatures (<310 K) where the unfolded state is only minimally populated (<0.5% from far-UV CD two-state fit estimates). This raises the question of whether Cnu populates a third state (i.e., a macroscopic three-state system) and whether this state is in equilibrium with the fully folded state over a thermodynamic barrier. Global three-state fits to the unfolding curves from six different experiments do result in reasonable fits but with crossing baselines for DSC; they are also inconclusive due to the numerous parameters employed, poorly determined baselines for the intermediate state (as the third state, if any, is less defined spectroscopically) and the associated prediction of cold-denaturation that is not observed experimentally. Independent lines of evidence from the semiquantitative WSME model (that is able to reproduce the DSC profile very well) and the qualitative coarse-grained MD simulations point to either a gradual melting of the fourth helix over zero thermodynamic barrier in the native ensemble or a continuously moving native ensemble, respectively. The rest of the structure unfolds over a marginal thermodynamic barrier at the midpoint (Figure 4C, 7C).

The molecular origin of the tunable structural heterogeneity arises from the unique conformational behavior of the fourth helix and the associated loop that unfolds gradually (over a negligible thermodynamic barrier, if any). We find strong evidence for this from the thermal melts of Cnu probed by near-UV CD (Figure 3C), fluorescence QY (particularly when comparing with the reference disordered C-pep; Figure 3E) and anisotropy (Figure 3F). We present direct confirmation of the temperature dependent structural heterogeneity in the C-terminal region of Cnu through NMR (Figure 6), coarse-grained and all-atom MD simulations (Figure 7). The lack of significant structural changes in the pretransition of far-UV CD is however surprising (Figure 2C). This signal is however challenging to interpret due to two reasons: short fourth helix and the presence of both tyrosine (Y69) and tryptophan (W67) within this helix that exhibit a near-perfect compensation of signals in the far-UV CD region when in helical conformation.[67] The slow exchange of different W67 resonances from NMR at low temperatures (slow dynamics) suggests that the multiple long-lived states in the broad native ensemble of Cnu exchange populations in a coordinate orthogonal to the folding direction. This possibly arises from non-native interactions of W67 with positively charged residues on the solvent-exposed face of helices 2 and 3 through cation-π interactions (residues K21, R41, R46, R47, R55 and K64). Extremely slow dynamics arising from non-native ionic interactions have in fact been reported in several proteins[68−70] lending strength to our interpretation, which needs to be experimentally tested. We are currently pursuing this avenue through mutational studies involving W67 and more directly through modulations of ionic strength conditions that can tune the strength of cation-π interactions.

The NMR model of Cnu at 298 K indicates partially structured fourth helix[11] validating our observations that predict the protein to be fully folded only at temperatures well below 285 K (note the well-defined near-UV CD spectrum in Figure 2B at 278 K). It is important to note that the same fourth helix is reasonably well folded in its homologues Hha and YmoA at 298 K (all NMR structures were solved in the absence of the binding partner H-NS).[9,10] This difference in the conformational behavior is possibly because of the fact that the loop connecting the third helix to the fourth is longer by 3 residues in Cnu with 2 glycines and a glutamine, compared to Hha and YmoA (Figure S9). This allows for larger conformational flexibility that potentially weakens the nonlocal interactions formed with the C-terminal half of the third helix in a strongly temperature dependent manner. This statement is supported by the smaller heteronuclear NOEs (hnNOE) and ^{15}N transverse relaxation rates (R_2) observed for the loop region compared to the folded part of the structure at 298 K; the fourth helix by itself exhibits high hnNOE and R_2 suggestive of partial structure in this region either from local or nonlocal interactions.[11]

Hha, that has a shorter loop, does not exhibit either of above features. However, positive temperature coefficients of chemical shifts have been reported for specific residues in the third and fourth helix indicative of a dynamic equilibrium between alternate conformations.[9] In an independent experiment involving the structural ensemble analysis of the YmoA SAXS profile, a certain degree of flexibility had to be explicitly included in the loop region connecting the third and fourth helix even at 285 K.[13] These observations taken together with our experimental and computational findings highlight that conformational dynamics and partial disorder in the loop and the fourth helix could be a conserved feature of the Hha family members. This is possibly the reason why the different structures of the Hha-family exhibit high RMSD in the region following the third helix (Figure 1).

The transcription regulation of virulence genes involves a complex three-component system with interactions between Cnu, H-NS dimer (minimal unit of ~260 residues) and curved DNA. Interestingly, it is the third and fourth helices of Hha/

DOI: 10.1021/jacs.6b10608
J. Am. Chem. Soc. 2017, 139, 792−802

YmoA/Cnu that serve as the binding site for the dimeric H-NS.[12,13] The interface of the complex is stabilized by an array of salt bridges termed as the charge zipper with the core of the complex stabilized by a cation-π interaction between the W68 in Hha (W67 in the fourth helix of Cnu) and K32 in H-NS. H-NS by itself displays a temperature-sensitive oligomeric status[71−73] whose null mutants can be rescued by Hha-like proteins suggesting that they can substitute for H-NS in the oligomers.[74] However, the binding affinity of H-NS to DNA does not change significantly between 283 and 310 K (∼150−400 μM).[72] Given these observations and since Cnu exhibits temperature modulated structural polymorphism in precisely the binding helices, it is possible that Cnu or Hha-like proteins allosterically modulate the stability and the intrinsic dynamics of the H-NS−DNA complex thus promoting or repressing expression of virulence genes.[75,76] Our results together with recent experiments that point to a H-NS independent role of the Hha-family[77] open up new frontiers in assessing the thermosensing mechanisms prevalent in enterobacteria.

From a folding-mechanistic viewpoint, graded structural polymorphism in the native ensemble is a feature that is consistently observed across all downhill folding proteins (i.e., molecular rheostat-like behavior[27,78]). While it has been argued before that large structural fluctuations in the native ensemble are intrinsic properties of mesoscale protein chains (and not just downhill folders),[58] it has been challenging to discern them from ensemble measurements. In this case, however, it is clear that Cnu exhibits substantial polymorphism in the native ensemble. The rheostat-like behavior with temperature arises from the requirement that it is structurally sensitive to temperature changes in the physiological range to regulate functional response. Our work is therefore further confirmation that functional determinants govern the folding mechanistic behavior of proteins.[79−82]

Recent studies have highlighted how disorder and downhill folding form a spectrum of possible "folding" mechanisms accessible to single-domain proteins.[23,83,84] On the other hand, Cnu exhibits a conformational behavior at precisely the boundary between these two regimes highlighting a novel unfolding mechanism that has not been observed before: the region following the third helix displays graded disorder while the structural scaffold involving the first three helices unfold over a marginal thermodynamic barrier. Our work shows that a continuous unfolding mechanism proposed for protein systems (i.e., globally downhill) need not encompass the entire structure, but can be restricted to even specific protein structural modules. In the case of Cnu, this seems to arise from a combination of weak packing of the fourth helix and the excess conformational flexibility of the long loop preceding it.

It is important to note that the extent to which the structure melts within the physiological temperature range in each of the Hha-family members could be different and determined by the specific amino acid differences. We are currently exploring this phenomenon in the homologues of Cnu, which is expected to shed more light on the molecular origins of thermosensing. This opens up the possibility of using Hha-family members as druggable targets to control infection, since interfering with the thermosensing mechanism will effectively eliminate the expression of virulence genes.

■ ASSOCIATED CONTENT

Supporting Information

The Supporting Information is available free of charge on the ACS Publications website at DOI: 10.1021/jacs.6b10608.

First-derivative analysis and two-state fit of Cnu fluorescence quantum yield, far-UV CD of the disordered C-pep, DSC baseline reproducibility and reversibility of the Cnu heat capacity profile, comparison of Cnu and Ubq DSC thermograms, global two-state, three-state and variable-barrier model fits, MD simulation trajectories, multiple sequence alignment of the Hha protein family (PDF)

■ AUTHOR INFORMATION

Corresponding Author

*athi@iitm.ac.in

ORCID

Athi N. Naganathan: 0000-0002-1655-7802

Notes

The authors declare no competing financial interest.

■ ACKNOWLEDGMENTS

We thank Mrityunjay Singh for help with the spectroscopic measurements, Karina Herrera-Guzman for help with NMR samples preparation and preliminary NMR measurements, and Soundhararajan Gopi for Figure 7B,G. The authors acknowledge the FIST facility sponsored by the Department of Science and Technology (DST), India at the Department of Biotechnology, IITM for the high-end instrumentation and Prof. Jayant Udgaonkar (NCBS, Bangalore, India) for extending his lab facilities for use. We also thank Prof. Miquel Pons and Dr. Jesús García for the clones of Cnu. A.N.N. is a recipient of the Wellcome Trust/DBT India Alliance Intermediate Fellowship. This work was supported by the grant BT/06/IYBA/2012−14 to A.N.N. from the Department of Biotechnology (DBT), New Delhi, India. The NMR instrumentation used in this work was supported in part by NSF grant DBI1040158 to D.F.

■ REFERENCES

(1) Steinmann, R.; Dersch, P. *Future Microbiol.* **2013**, *8*, 85−105.
(2) Hurme, R.; Rhen, M. *Mol. Microbiol.* **1998**, *30*, 1−6.
(3) Klinkert, B.; Narberhaus, F. *Cell. Mol. Life Sci.* **2009**, *66*, 2661−2676.
(4) Narayan, S.; Kombrabail, M. H.; Das, S.; Singh, H.; Chary, K. V.; Rao, B. J.; Krishnamoorthy, G. *Nucleic Acids Res.* **2015**, *43*, 493−503.
(5) Hurme, R.; Berndt, K. D.; Namork, E.; Rhen, M. *J. Biol. Chem.* **1996**, *271*, 12626−12631.
(6) Kamp, H. D.; Higgins, D. E. *PLoS Pathog.* **2011**, *7*, e1002153.
(7) Nieto, J. M.; Carmona, M.; Bolland, S.; Jubete, Y.; de la Cruz, F.; Juarez, A. *Mol. Microbiol.* **1991**, *5*, 1285−1293.
(8) Mourino, M.; Madrid, C.; Balsalobre, C.; Prenafeta, A.; Munoa, F.; Blanco, J.; Blanco, M.; Blanco, J. E.; Juarez, A. *Infect. Immun.* **1996**, *64*, 2881−2884.
(9) Garcia, J.; Cordeiro, T. N.; Nieto, J. M.; Pons, I.; Juarez, A.; Pons, M. *Biochem. J.* **2005**, *388*, 755−762.
(10) McFeeters, R. L.; Altieri, A. S.; Cherry, S.; Tropea, J. E.; Waugh, D. S.; Byrd, R. A. *Biochemistry* **2007**, *46*, 13975−13982.
(11) Bae, S.-H.; Liu, D.; Lim, H. M.; Lee, Y.; Choi, B.-S. *Biochemistry* **2008**, *47*, 1993−2001.
(12) Ali, S. S.; Whitney, J. C.; Stevenson, J.; Robinson, H.; Howell, P. L.; Navarre, W. W. *J. Biol. Chem.* **2013**, *288*, 13356−13369.

DOI: 10.1021/jacs.6b10608
J. Am. Chem. Soc. 2017, 139, 792−802

(13) Cordeiro, T. N.; Garcia, J.; Bernado, P.; Millet, O.; Pons, M. *J. Biol. Chem.* **2015**, *290*, 21200−21212.
(14) Nieto, J. M.; Mourino, M.; Balsalobre, C.; Madrid, C.; Prenafeta, A.; Munoa, F. J.; Juarez, A. *FEMS Microbiol. Lett.* **1997**, *155*, 39−44.
(15) Juarez, A.; Nieto, J. M.; Prenafeta, A.; Miquelay, E.; Balsalobre, C.; Carrascal, M.; Madrid, C. *Adv. Exp. Med. Biol.* **2000**, *485*, 127−131.
(16) Atlung, T.; Ingmer, H. *Mol. Microbiol.* **1997**, *24*, 7−17.
(17) Stoebel, D. M.; Free, A.; Dorman, C. J. *Microbiology* **2008**, *154*, 2533−2545.
(18) White-Ziegler, C. A.; Davis, T. R. *J. Bacteriol.* **2009**, *191*, 1106−1110.
(19) Nieto, J. M.; Madrid, C.; Prenafeta, A.; Miquelay, E.; Balsalobre, C.; Carrascal, M.; Juarez, A. *Mol. Gen. Genet.* **2000**, *263*, 349−358.
(20) Madrid, C.; Nieto, J. M.; Juarez, A. *Int. J. Med. Microbiol.* **2002**, *291*, 425−432.
(21) Kim, D. E.; Chivian, D.; Baker, D. *Nucleic Acids Res.* **2004**, *32*, W526−W531.
(22) Jackson, M. W.; Silva-Herzog, E.; Plano, G. V. *Mol. Microbiol.* **2004**, *54*, 1364−1378.
(23) Muñoz, V.; Campos, L. A.; Sadqi, M. *Curr. Opin. Struct. Biol.* **2016**, *36*, 58−66.
(24) Jackson, S. E.; Fersht, A. R. *Biochemistry* **1991**, *30*, 10428−10435.
(25) Baldwin, R. L. *Annu. Rev. Biophys.* **2008**, *37*, 1−21.
(26) Udgaonkar, J. B. *Annu. Rev. Biophys.* **2008**, *37*, 489−510.
(27) Garcia-Mira, M. M.; Sadqi, M.; Fischer, N.; Sanchez-Ruiz, J. M.; Muñoz, V. *Science* **2002**, *298*, 2191−2195.
(28) Gruebele, M. *C. R. Biol.* **2005**, *328*, 701−712.
(29) Naganathan, A. N.; Doshi, U.; Fung, A.; Sadqi, M.; Muñoz, V. *Biochemistry* **2006**, *45*, 8466−8475.
(30) Muñoz, V. *Annu. Rev. Biophys. Biomol. Struct.* **2007**, *36*, 395−412.
(31) Bhuyan, A. K.; Udgaonkar, J. B. *Biochemistry* **1999**, *38*, 9158−9168.
(32) Larios, E.; Li, J. S.; Schulten, K.; Kihara, H.; Gruebele, M. *J. Mol. Biol.* **2004**, *340*, 115−125.
(33) Ma, H. R.; Gruebele, M. *Proc. Natl. Acad. Sci. U. S. A.* **2005**, *102*, 2283−2287.
(34) Fung, A.; Li, P.; Godoy-Ruiz, R.; Sanchez-Ruiz, J. M.; Muñoz, V. *J. Am. Chem. Soc.* **2008**, *130*, 7489−7495.
(35) Jha, S. K.; Dasgupta, A.; Malhotra, P.; Udgaonkar, J. B. *Biochemistry* **2011**, *50*, 3062−3074.
(36) Sarkar, S. S.; Udgaonkar, J. B.; Krishnamoorthy, G. *Biophys. J.* **2013**, *105*, 2392−2402.
(37) Naganathan, A. N.; Muñoz, V. *J. Phys. Chem. B* **2014**, *118*, 8982−8994.
(38) Kubelka, G. S.; Kubelka, J. *J. Am. Chem. Soc.* **2014**, *136*, 6037−6048.
(39) Lai, J. K.; Kubelka, G. S.; Kubelka, J. *Proc. Natl. Acad. Sci. U. S. A.* **2015**, *112*, 9890−9895.
(40) Kim, M. S.; Bae, S. H.; Yun, S. H.; Lee, H. J.; Ji, S. C.; Lee, J. H.; Srivastava, P.; Lee, S. H.; Chae, H.; Lee, Y.; Choi, B. S.; Chattoraj, D. K.; Lim, H. M. *J. Bacteriol.* **2005**, *187*, 6998−7008.
(41) Paytubi, S.; Madrid, C.; Forns, N.; Nieto, J. M.; Balsalobre, C.; Uhlin, B. E.; Juarez, A. *Mol. Microbiol.* **2004**, *54*, 251−263.
(42) Wako, H.; Saito, N. *J. Phys. Soc. Jpn.* **1978**, *44*, 1939−1945.
(43) Muñoz, V.; Eaton, W. A. *Proc. Natl. Acad. Sci. U. S. A.* **1999**, *96*, 11311−11316.
(44) Naganathan, A. N. *J. Chem. Theory Comput.* **2012**, *8*, 4646−4656.
(45) Naganathan, A. N. *J. Phys. Chem. B* **2013**, *117*, 4956−4964.
(46) Rajasekaran, N.; Gopi, S.; Narayan, A.; Naganathan, A. N. *J. Phys. Chem. B* **2016**, *120*, 4341−4350.
(47) Noel, J. K.; Whitford, P. C.; Sanbonmatsu, K. Y.; Onuchic, J. N. *Nucleic Acids Res.* **2010**, *38*, W657−W661.
(48) Pronk, S.; Pall, S.; Schulz, R.; Larsson, P.; Bjelkmar, P.; Apostolov, R.; Shirts, M. R.; Smith, J. C.; Kasson, P. M.; van der Spoel, D.; Hess, B.; Lindahl, E. *Bioinformatics* **2013**, *29*, 845−854.
(49) Naganathan, A. N.; De Sancho, D. *J. Phys. Chem. B* **2015**, *119*, 14925−14933.
(50) Strickland, E. H. *CRC Crit. Rev. Biochem.* **1974**, *2*, 113−175.
(51) Robertson, A. D.; Murphy, K. P. *Chem. Rev.* **1997**, *97*, 1251−1267.
(52) Naganathan, A. N.; Perez-Jimenez, R.; Sanchez-Ruiz, J. M.; Muñoz, V. *Biochemistry* **2005**, *44*, 7435−7449.
(53) Lakowicz, J. R. *Principles of Fluoresence Spectroscopy*; Springer: New York, USA, 2007.
(54) Muñoz, V.; Sanchez-Ruiz, J. M. *Proc. Natl. Acad. Sci. U. S. A.* **2004**, *101*, 17646−17651.
(55) Liu, F.; Gruebele, M. *J. Mol. Biol.* **2007**, *370*, 574−584.
(56) Sanchez-Ruiz, J. M. *Annu. Rev. Phys. Chem.* **2011**, *62*, 231−255.
(57) Naganathan, A. N.; Perez-Jimenez, R.; Muñoz, V.; Sanchez-Ruiz, J. M. *Phys. Chem. Chem. Phys.* **2011**, *13*, 17064−17076.
(58) Cooper, A. *Proc. Natl. Acad. Sci. U. S. A.* **1976**, *73*, 2740−2741.
(59) Johnson, C. M. *Arch. Biochem. Biophys.* **2013**, *531*, 100−109.
(60) Guzman-Casado, M.; Parody-Morreale, A.; Robic, S.; Marqusee, S.; Sanchez-Ruiz, J. M. *J. Mol. Biol.* **2003**, *329*, 731−743.
(61) Ibarra-Molero, B.; Naganathan, A. N.; Sanchez-Ruiz, J. M.; Muñoz, V. *Methods Enzymol.* **2016**, *567*, 281−318.
(62) Gomez, J.; Hilser, V. J.; Xie, D.; Freire, E. *Proteins: Struct., Funct., Genet.* **1995**, *22*, 404−412.
(63) Thomas, S. T.; Makhatadze, G. I. *Biochemistry* **2000**, *39*, 10275−10283.
(64) Lebowitz, J.; Lewis, M. S.; Schuck, P. *Protein Sci.* **2002**, *11*, 2067−2079.
(65) Erickson, H. P. *Biol. Proced. Online* **2009**, *11*, 32−51.
(66) Naganathan, A. N. *WIREs Comput. Mol. Sci.* **2013**, *3*, 504−514.
(67) Chakrabartty, A.; Kortemme, T.; Padmanabhan, S.; Baldwin, R. L. *Biochemistry* **1993**, *32*, 5560−5565.
(68) Waldauer, S. A.; Bakajin, O.; Lapidus, L. J. *Proc. Natl. Acad. Sci. U. S. A.* **2010**, *107*, 13713−13717.
(69) Voelz, V. A.; Jager, M.; Yao, S. H.; Chen, Y. J.; Zhu, L.; Waldauer, S. A.; Bowman, G. R.; Friedrichs, M.; Bakajin, O.; Lapidus, L. J.; Weiss, S.; Pande, V. S. *J. Am. Chem. Soc.* **2012**, *134*, 12565−12577.
(70) Chung, H. S.; Piana-Agostinetti, S.; Shaw, D. E.; Eaton, W. A. *Science* **2015**, *349*, 1504−1510.
(71) Smyth, C. P.; Lundback, T.; Renzoni, D.; Siligardi, G.; Beavil, R.; Layton, M.; Sidebotham, J. M.; Hinton, J. C.; Driscoll, P. C.; Higgins, C. F.; Ladbury, J. E. *Mol. Microbiol.* **2000**, *36*, 962−972.
(72) Ono, S.; Goldberg, M. D.; Olsson, T.; Esposito, D.; Hinton, J. C.; Ladbury, J. E. *Biochem. J.* **2005**, *391*, 203−213.
(73) Arold, S. T.; Leonard, P. G.; Parkinson, G. N.; Ladbury, J. E. *Proc. Natl. Acad. Sci. U. S. A.* **2010**, *107*, 15728−15732.
(74) Rodriguez, S.; Nieto, J. M.; Madrid, C.; Juarez, A. *J. Bacteriol.* **2005**, *187*, 5452−5459.
(75) Fernandez-de-Alba, C.; Berrow, N. S.; Garcia-Castellanos, R.; Garcia, J.; Pons, M. *J. Mol. Biol.* **2013**, *425*, 2347−2358.
(76) Renault, M.; Garcia, J.; Cordeiro, T. N.; Baldus, M.; Pons, M. *FEBS J.* **2013**, *280*, 2916−2928.
(77) Solorzano, C.; Srikumar, S.; Canals, R.; Juarez, A.; Paytubi, S.; Madrid, C. *Front. Microbiol.* **2015**, *6*, 773.
(78) Cerminara, M.; Desai, T. M.; Sadqi, M.; Muñoz, V. *J. Am. Chem. Soc.* **2012**, *134*, 8010−8013.
(79) Whitford, P. C.; Onuchic, J. N. *Curr. Opin. Struct. Biol.* **2015**, *30*, 57−62.
(80) Naganathan, A. N.; Sanchez-Ruiz, J. M.; Munshi, S.; Suresh, S. *J. Phys. Chem. B* **2015**, *119*, 1323−1333.
(81) Munshi, S.; Naganathan, A. N. *Phys. Chem. Chem. Phys.* **2015**, *17*, 11042−11052.
(82) Giri Rao, V. H.; Gosavi, S. *Curr. Opin. Struct. Biol.* **2016**, *36*, 67−74.
(83) Naganathan, A. N.; Orozco, M. *J. Am. Chem. Soc.* **2011**, *133*, 12154−12161.
(84) Wang, Y.; Chu, X.; Longhi, S.; Roche, P.; Han, W.; Wang, E.; Wang, J. *Proc. Natl. Acad. Sci. U. S. A.* **2013**, *110*, E3743−3752.

DOI: 10.1021/jacs.6b10608
J. Am. Chem. Soc. 2017, 139, 792−802